ADVANCED FUNCTIONAL MATERIALS
www.afm-journal.de

Multifunctional Bioinstructive 3D Architectures to Modulate Cellular Behavior

*Jayasheelan Vaithilingam, Paola Sanjuan-Alberte, Simona Campora, Graham A. Rance, Long Jiang, Jordan Thorpe, Laurence Burroughs, Christopher J. Tuck, Chris Denning, Ricky D. Wildman, Richard J. M. Hague, Morgan R. Alexander, and Frankie J. Rawson**

Biological structures control cell behavior via physical, chemical, electrical, and mechanical cues. Approaches that allow us to build devices that mimic these cues in a combinatorial way are lacking due to there being no suitable instructive materials and limited manufacturing procedures. This challenge is addressed by developing a new conductive composite material, allowing for the fabrication of 3D biomimetic structures in a single manufacturing method based on two-photon polymerization. The approach induces a combinatorial biostimulative input that can be tailored to a specific application. Development of the 3D architecture is performed with a chemically actuating photocurable acrylate previously identified for cardiomyocyte attachment. The material is made conductive by impregnation with multiwalled carbon nanotubes. The bioinstructive effect of 3D nano- and microtopography is combined with electrical stimulation, incorporating biochemical, and electromechanical cues to stimulate cells in serum-free media. The manufactured architecture is combined with cardiomyocytes derived from human pluripotent stem cells. It is demonstrated that by mimicking biological occurring cues, cardiomyocyte behavior can be modulated. This represents a step change in the ability to manufacture 3D multifunctional biomimetic modulatory architectures. This platform technology has implications in areas spanning regenerative medicine, tissue engineering to biosensing, and may lead to more accurate models for predicting toxicity.

1. Introduction

Nature constructs microscopic hierarchical cellular machines and architectures or niches that have defined bimolecular, chemical, mechanical, and electrical properties, which provide cues to enable modulation of differentiation and maturation of cells. For example, cardiac tissue instructs cardiomyocytes to have aligned myofibrils and elongated sarcomeres.[1] In order to develop systems that simulate biology, we need devices that mimic these niches by providing the equivalent signaling mechanism to control cellular behavior. Signaling methods typically used in vitro to modulate cell behavior include gene manipulation,[2] biomaterial chemistry,[3] surface topography,[4] biochemical signaling,[5] and electromechanical stimulation,[6] which affect growth-promoting factors.[7] While most of the reported methods have focused on one or two of these, achieving some success,[7b,8] a combination of all these stimuli is desirable to mimic physiological conditions more accurately.

Dr. J. Vaithilingam, Dr. P. Sanjuan-Alberte, Prof. C. J. Tuck, Prof. R. D. Wildman, Prof. R. J. M. Hague
Centre for Additive Manufacturing
Faculty of Engineering
University of Nottingham
Nottingham NG8 1BB, UK

Dr. P. Sanjuan-Alberte, Dr. F. J. Rawson
Regenerative Medicine and Cellular Therapies
School of Pharmacy
University of Nottingham
Nottingham NG7 2RD, UK
E-mail: Frankie.Rawson@nottingham.ac.uk

Dr. S. Campora
Scienze e Tecnologie Biologiche
Chimiche e Farmaceutiche (STEBICEF)
University of Palermo
Viale delle Scienze Ed. 16, 90128 Palermo, Italy

The ORCID identification number(s) for the author(s) of this article can be found under https://doi.org/10.1002/adfm.201902016.

DOI: 10.1002/adfm.201902016

Dr. S. Campora
ABIEL S.r.l.
c/o Arca Incubatore di Imprese
Viale delle Scienze Ed. 16, 90128 Palermo, Italy

Dr. G. A. Rance
Nanoscale and Microscale Research Centre
University of Nottingham
Nottingham NG7 2RD, UK

Dr. L. Jiang, J. Thorpe, Dr. L. Burroughs, Prof. M. R. Alexander
Advanced Materials and Healthcare Technologies
School of Pharmacy
University of Nottingham
Nottingham NG7 2RD, UK

J. Thorpe, Prof. C. Denning
Department of Stem Cell Biology
Faculty of Medicine & Health Sciences
University of Nottingham
Nottingham NG7 2RD, UK

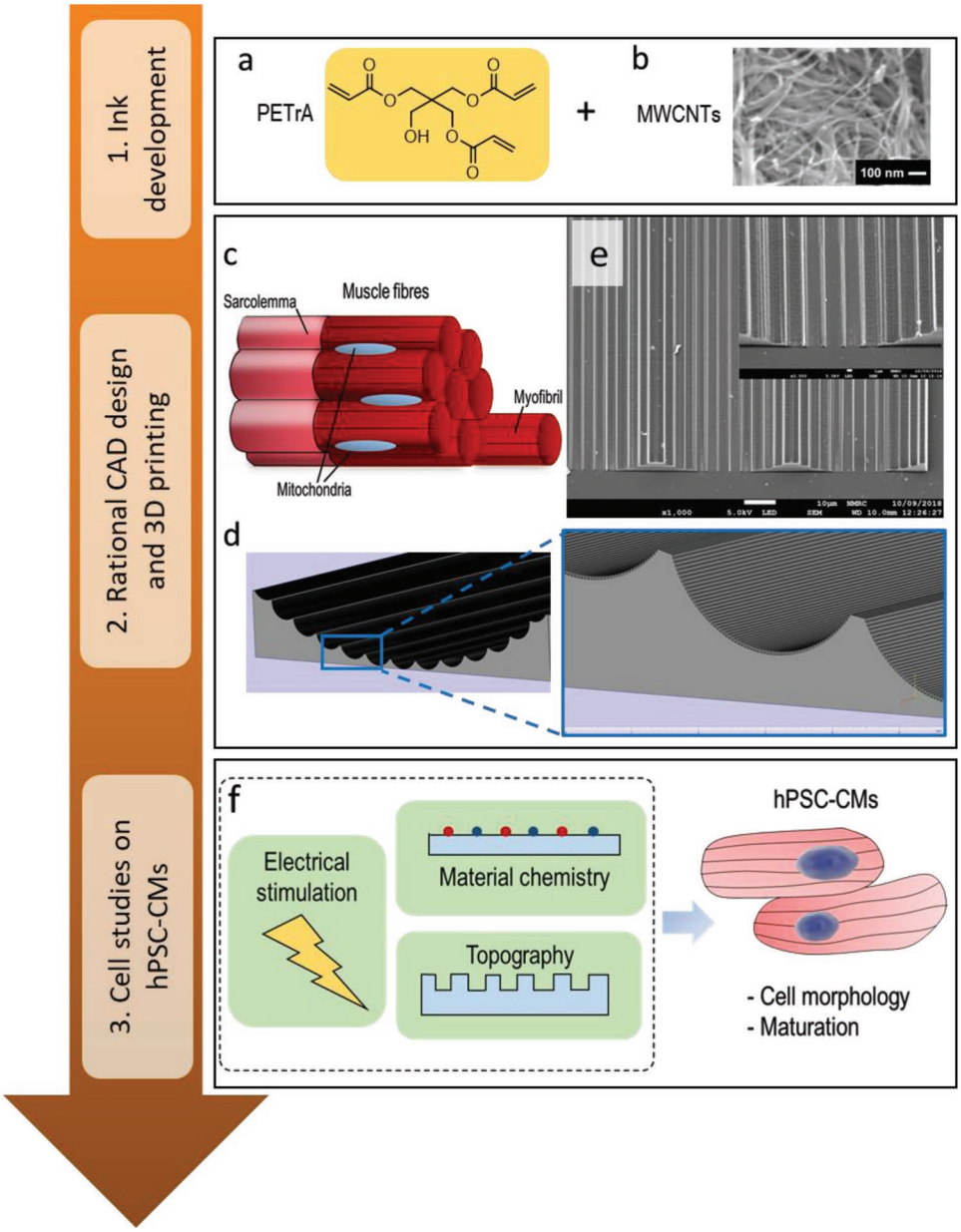

Figure 1. Process followed for rational ink development, 3D printing, and stimulation of human-induced stem cell derived cardiomyocytes (hPSC-CMs). 1) Inks were developed using a) pentaerythritol triacrylate (PETrA). Conductive inks were developed by modification of PETrA with b) multiwalled carbon nanotubes (MWCNTs). 2) Rational 3D design was inspired on c) in vivo structure of stacked myofibrils. d) Computer-aided design (CAD) model of 3D myofibril-like structures with nano/microtopographies. e) SEM image of 3D printed myofibril-like structures using PETrA ink. 3) Cell studies were carried out by combination of physical and mechanical cues provided by f) electrical stimulation, material chemistry, and material topography on hPSC-CMs.

Cardiomyocyte-promoting acrylic polymers screened by high-throughput methods have been identified in previous studies,[3] demonstrating that the chemical composition of the materials can enhance human pluripotent stem cell-derived cardiomyocyte (hPSC-CMs) development. This method was used to select pentaerythritol triacrylate (PETrA) (**Figure 1**a) from the screening of polymer microarrays. Electrical properties of materials have also been shown to have a modulatory effect.[9] PETrA's electrical properties were tuned using a dispersion of conductive multiwalled carbon nanotubes (MWCNTs) (Figure 1b) into PETrA in order to make this material electroactive, and it is the first example of this material being modified to improve its electrical properties.

Biomimetic 3D structures may aid in offering the correct cellular instructions to enable us to modulate cellular behavior that better resembles human tissues.[10] Digital 3D-printing techniques enable the engineering of materials with tunable mechanical,

chemical, and electrical properties.[11] Although extrusion 3D-printers have often been used for bioprinting,[12] this technique is limited to the production of features of >50 micrometers in diameter, significantly bigger than the submicron scales required for mimicking biological structures as exemplified in heart tissue (Figure 1c,d). Two-photon polymerization (2PP) is a laser-induced photopolymerization technique and has been shown to direct construction of biomimetic constructs at submicron scales (≈70 nm resolution) without requiring support structures.[13] PETrA has been studied in the manufacturing of micro- and nanostructures using the 2PP process for various applications.[13,14] 2PP has been used to produce acrylic polymer and hydrogel constructs and utilized with neuronal and retinal cells.[15] However, no 2PP produced structures incorporating PETrA have been used for bio-instructive applications. We used the 2PP method to fabricate biomimetic structures spanning the macro-nanoscales (Figure 1e) to modulate cardiomyocytes behavior derived from hPSC-CMs. Details and description of the hPSC-CMs used can be found elsewhere.[16]

Herein, we report PETrA as a promising material in the manufacturing of 3D biomimetic constructs that allows for a combination of electromechanical stimulation. These different types of cues can be simultaneously applied, demonstrating the multifunctionality of the printed structures (Figure 1f). Differentiation of hPSCs to cardiomyocytes was performed using a previous procedure[16] (Figure S1, Supporting Information) and the purity of the obtained cardiomyocyte population was > 90% by expression of the cardiac marker troponin TNNI3 (Figure S2, Supporting Information). PETrA and composite mixtures of PETrA with MWCNTs (PETrA+MWCNTs) inks were formulated for subsequent 3D printing by 2PP. In order to optimize the ink formulations and characterize the printed structures, four parameters were assessed: i) degree of conversion (DC), ii) impact on cell viability, iii) electrical conductivity, and iv) stiffness of the printed structures. Cardiomyocyte behaviour was then assessed in these biomimetic scaffolds by analysis of cell morphology and sarcomere length.

2. Results and Discussion

2.1. Ink Formulation

Irgacure 369 was used as a photoinitiator (PI) to enable free-radical polymerization of the acrylic monomer.[17] An increase in PI concentration is known to increase the DC of monomer to polymer and reducing the fabrication time.[18] Conversely, the increase in PI was previously noted to affect the cell viability due to cytotoxicity as gauged by cell proliferation assays.[19] To assess this in detail, structures were 2PP-printed using a range of PI concentrations including 0.5%, 1%, 2%, and 3% by weight. The DC was assessed using Raman spectroscopy and the viability of hPSC-CMs was assessed using a live/dead fluorescence assay (Figure S3, Supporting Information). More information on the calculation of DC can be found in the Supporting information. Since both the cell viability and the DC are of utmost importance to the present study, 1% was chosen as an optimal PI concentration to make structures for hPSC-CMs (**Figure 2**a,b). Additionally, in comparison with control surfaces, the PETrA surfaces were noted to promote cell adhesion featuring more cells on the surface (Figure S3, Supporting Information).

Composite mixtures of PETrA+MWCNTs were prepared with 0.2 wt% and 0.1 wt%, since the 2PP process requires transparent material so that the laser can pass through it (Figure 2c). Interestingly, the addition of MWCNTs decreased the DC with results showing more than a 50% reduction in the DC with a two-fold increase in MWCNT concentration. However, such DC using 2PP to fabricate microstructures containing carbon nanotubes has not been achieved until the data reported herein.[9c,20] Multispectral Raman imaging of the 2PP printed structures revealed a good dispersion of MWCNTs into the printed structure (Figure 2d). Cell viability was 54% and 87% on 0.2 wt% and 0.1 wt% MWCNTs composite structures, respectively (Figure 2a). These results indicate that since the DC was low (≈10.5%) for 0.2 wt% compared to 0.1 wt% MWCNTs concentration, the presence of residual monomer and the unreacted PI might have produced cytotoxic effects to the hPSC-CMs, affecting the cell viability. Based on the material characterization and cell viability assay, 0.1 wt% MWCNTs was used as the optimal concentration in the subsequent experiments.

Electrochemical characterization of the composite structures (0.1 wt% MWCNTs) was performed using electrochemical impedance spectroscopy. This revealed an improvement in the electrical conductivity of 2PP fabricated composite structures (Figure 2e) with a reduction in the impedance observed from 1 to 0.6 GΩ and tallies with previous reports of MWCNT based composite materials.[9b,21] The modulus of biomaterials is known to affect the formation of contractile apparatus in hPSC-CMs and in turn, the maturity of the cells.[22] A 68% increase in the modulus (obtained using atomic force microscopy) from 759 ± 22 MPa for PETrA to 989 ± 62 MPa for the composite material with 0.1 wt% MWCNTs was noted, indicating the addition of MWCNTs increased the modulus (Figure 2f).

2.2. Effect of Material and Topography on hPSC-CMs

After optimizing the printing and characterizing the structures, the ability to understand the impact of chemical, electromechanical and topographical cues on hPSC-CMs morphology was studied. This was done by assessing these cues individually and after a combinatorial approach.

Impact of nanotopographies on cell morphology was studied by measuring the cell aspect ratio and cell alignment. Mature cardiomyocytes have an aspect ratio of ≈7:1 and a high degree of alignment. This was performed on glass (control); flat (**Figure 3**a) and grooved (Figure 3b,c) pristine PETrA; and flat PETrA+MWCNTs composite structures. Grooved PETrA surfaces were noted to improve the alignment with angles <10° (****p) and yield a significantly higher aspect ratio (4:1) (****p) compared to cells on the flat surfaces (2:1) (Figure 3d–j). On control and flat PETrA surfaces, the hPSC-CMs featured polygonal shape with low aspect ratio as witnessed previously.[8a] Interestingly,

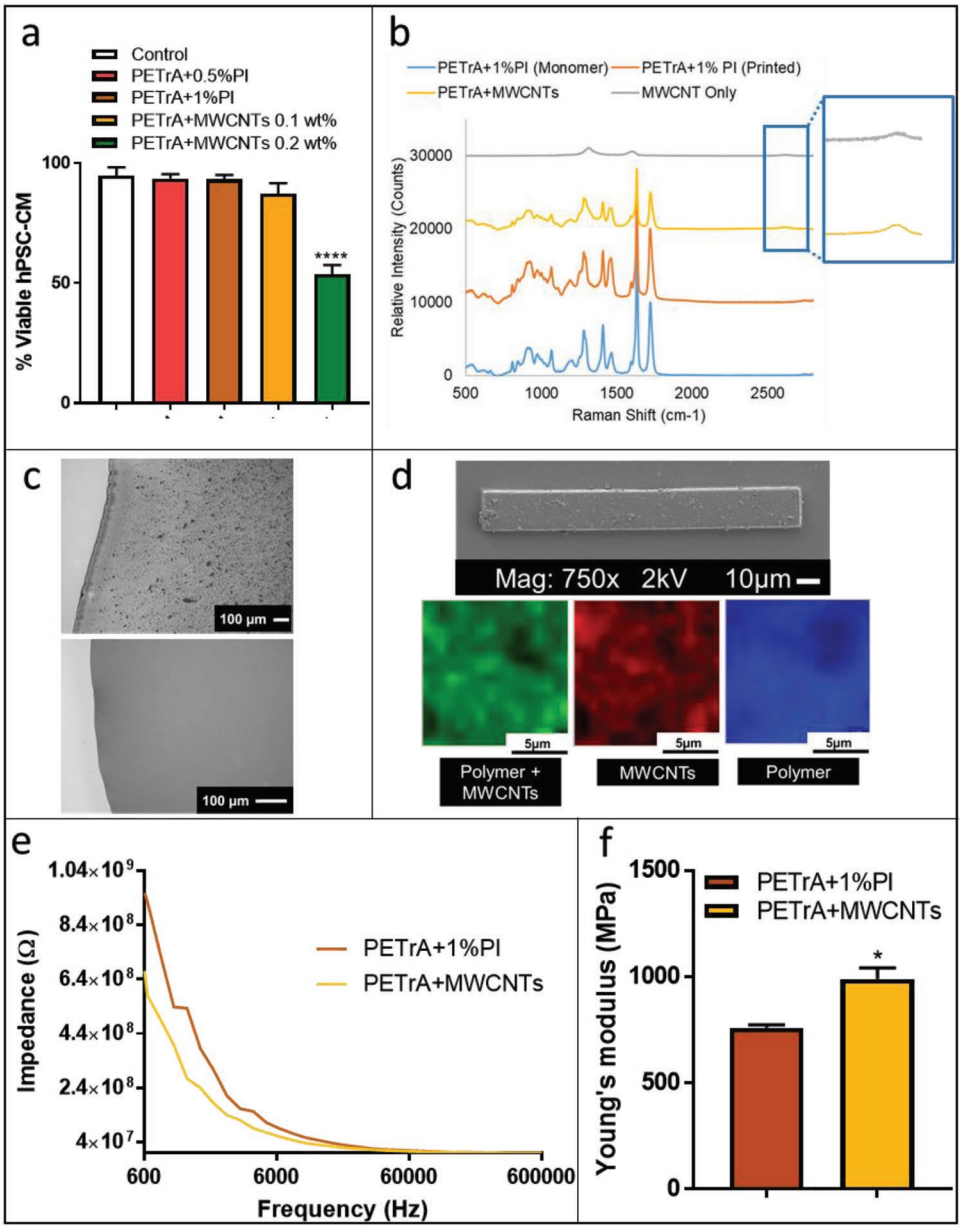

Figure 2. a) Viability of hPSC-CMs on different surfaces; b) Raman spectra obtained from the pristine PETrA ink, a printed structure using the pristine PETrA and PETrA+MWCNTs, and pristine MWCNTs; c) optical image of PETrA modified with MWCNTs (PETrA+MWCNTs) before (top) and after (bottom) centrifuging to remove agglomerated MWCNTs; d) a 3D printed composite structure with below images showing the Raman maps describing the distribution of MWCNTs and polymer in the print; e) electrical impedance of pristine PETrA and the composite; f) Young's modulus of the 3D printed structure using PETrA and the composite.

hPSC-CMs cultured on the flat PETrA+MWCNTs composite structures featured elongated cells with an aspect ratio of 3.75:1 (***p), significantly higher than the flat PETrA surface. As MWCNTs were randomly dispersed in the ink solution, this suggests that the composite increased the cell elongation due to the guidance provided by the random orientation of the fibrous structure of MWCNTs.[9a] At this stage, it was not possible to print nanotopographies using the PETrA+MWCNTs composite due to lack of resolution with this ink. From this, it can be seen that nanotopographies significantly affect the organization of the cells, as expected in native tissues.

Structural differences of the sarcomeres were also studied, as the length of sarcomeres vary with phenotypical changes. For instance, physiological values of sarcomere lengths of adult cardiomyocytes are around 2.2 µm, and immature sarcomeres have values of 1.6 µm.[23] These structural differences were determined by measuring the sarcomere

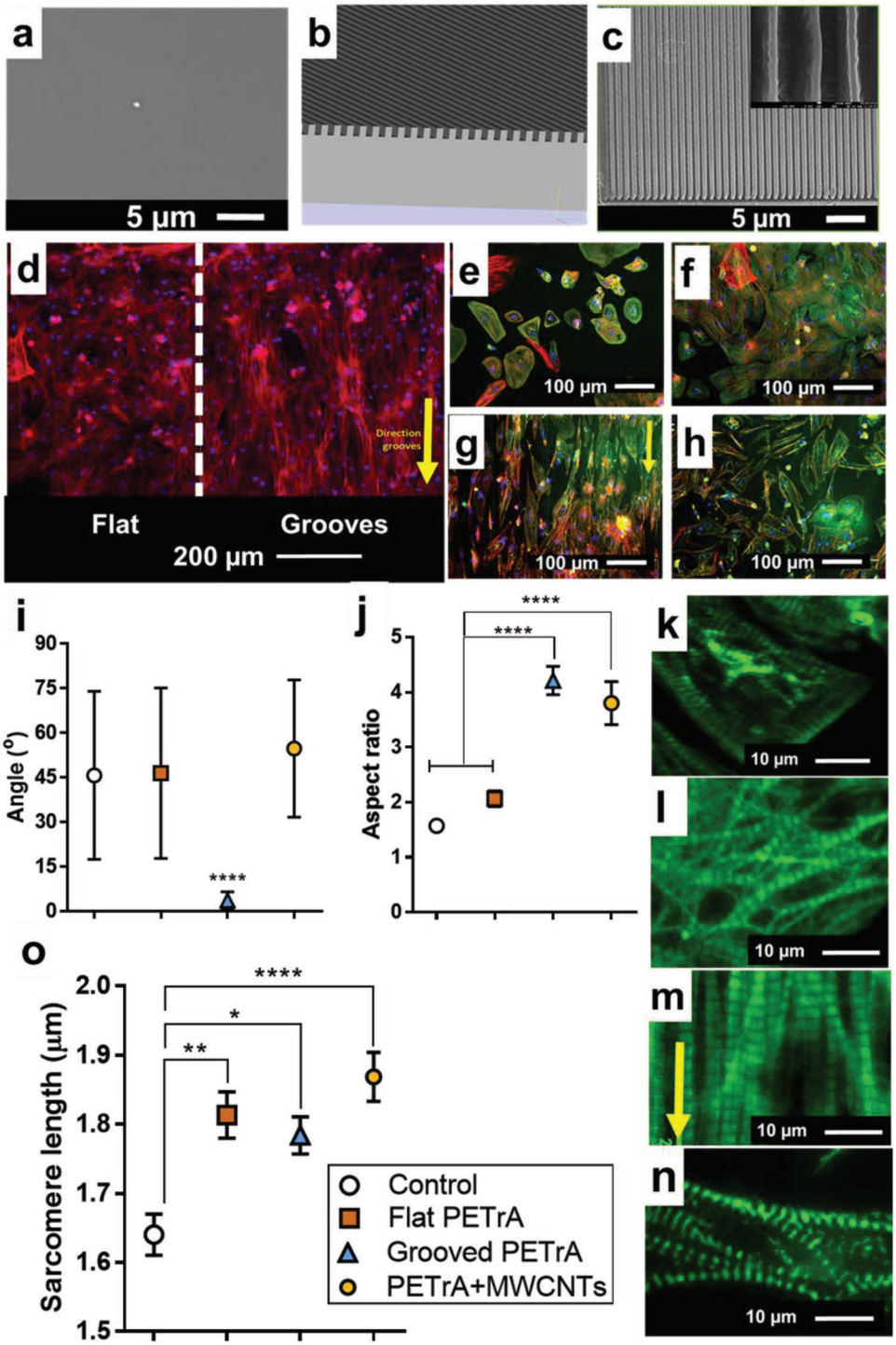

Figure 3. a) 3D printed PETrA surface (white dot shows a defect on the structure to highlight the flat topography); b) CAD design and c) printed surface with grooves; d) hPSC-CM directional alignment to the flat and grooved areas of a 3D printed PETrA surface (nuclei were staining with Hoechst staining (blue) and actin fibers with phalloidin (red)); hPSC-CMs attached on e) glass, f) flat, and g) grooved pristine PETrA surfaces and h) PETrA+MWCNTs composite surface; i) aspect ratio and j) alignment of hPSC-CMs on different surface topographies; fluorescence microscopy images of sarcomeres on k) control, l) flat PETrA, m) grooved PETrA, and n) flat PETrA+MWCNTs structures and o) their corresponding lengths. Sarcomeres were immunolabeled for alpha-actinin (green). Direction of grooves is indicated by yellow arrows.

length[3,24] as shown in Figure S4 (Supporting Information). The sarcomere images and lengths measured for different samples have been shown in Figure 3k–o. hPSC-CMs cultured on flat surfaces depicted disorganized myofibrils due to the polygonal morphology of the cells, whereas on the grooved PETrA structures and on the composite structure,

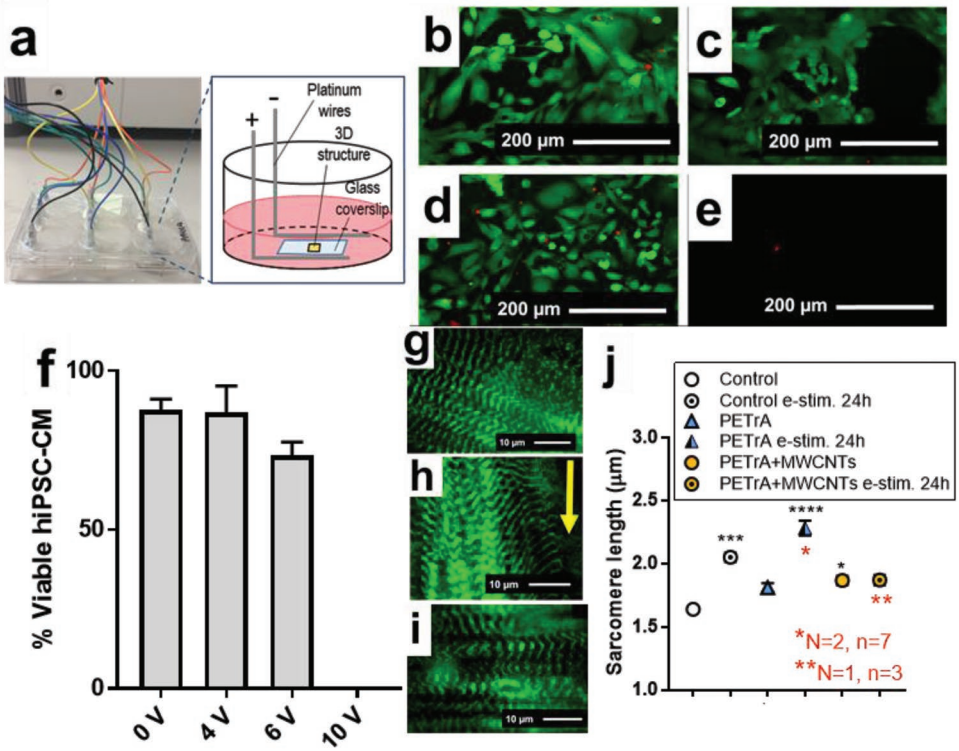

Figure 4. a) Bioreactor used to perform electrical stimulation; b) fluorescence microscopic images showing the viability of hPSC-CMs 7 d after electrical stimulation b) 0 V, c) 4 V, d) 6 V, e) 10 V, and (f) shows their corresponding percentage viability; fluorescence microscopic images of electrically stimulated hPSC-CMs immunostained for cardiac alpha-actinin on g) control, h) flat pristine grooved PETrA, i) PETrA+MWCNTs, and j) their corresponding sarcomere lengths after 24 h of electrical stimulation at 2 V and 3 Hz. Yellow arrow indicates the direction of grooves.

an organized myofibril with the parallel arrangement was observed. In terms of their sarcomere lengths, cells on the flat PETrA and grooved PETrA surfaces showed significantly longer sarcomeres (1.81 and 1.78 µm, respectively (**p, *p)) compared to the control (glass) surface (1.64 µm). The hPSC-CMs on the PETrA+MWCNTs structure also showed significantly longer sarcomeres (1.86 µm, ****p). This demonstrates our ability to control cellular morphology and intracellular components using different materials and nanotopographies. Our next aim was the study the effect of electrical stimulation, inherent in biology.[8b,25]

2.3. Electrical Stimulation hPSC-CMs

The electro-mechanical stimulus was provided wirelessly (without a physical wired connection of the electrodes to the 2PP structure) to hPSC-CMs using a modified 6 well cell culture plate enabling electrical stimulation as shown in **Figure 4**a.[26] The required electrical potential to stimulate the hPSC-CMs was previously optimized to obtain the excitation threshold (Figure S5, Supporting Information). Viability of the cells after electrical stimulation was studied by live/dead fluorescence assays to understand the impact of the applied electric potential (Figure 4b–f). The applied electric potential was kept to a minimum (2 V and 3 Hz) to prevent cell death. On applying this electric potential for 24 h, the level of organization of the myofibrils of electrically stimulated cells was higher (Figure 4g–i). On control (glass) surfaces, sarcomere lengths significantly increased to 2.05 µm (***p) (Figure 4j). Similarly, after electro-mechanical stimulation, the grooved PETrA displayed a sarcomere length of 2.28 µm (****p) similar to that measured for adult cardiomyocytes. The PETrA+MWCNTs structure did not exhibit a signification variation in the sarcomere length before or after electrical stimulation (1.87 µm). From this observation, we hypothesize that electrical stimulation could be one of the key drivers to control intracellular ultrastructure; however, topographical cues are still needed to control the cellular shape.

2.4. Combinatorial Approach of Multistimulation

Complex 3D structures with an enhanced topography can be used to mimic a particular tissue and fit the desired application. In this case, to demonstrate the capabilities of this technology, 3D structures were developed to resemble native myofibrils (Figure 1e). Structural design was optimized after preliminary studies (Figure S6, Supporting Information). Biomimetic myofibril-like structures were printed using 2PP in PETrA with and without MWCNTs (**Figure 5**a,b). The 3D topography, and bioinstructive material, allowing for biochemical and electromechanical cues were integrated into this design. On applying electrical stimulation to the 3D myofibril-like structure, the sarcomere

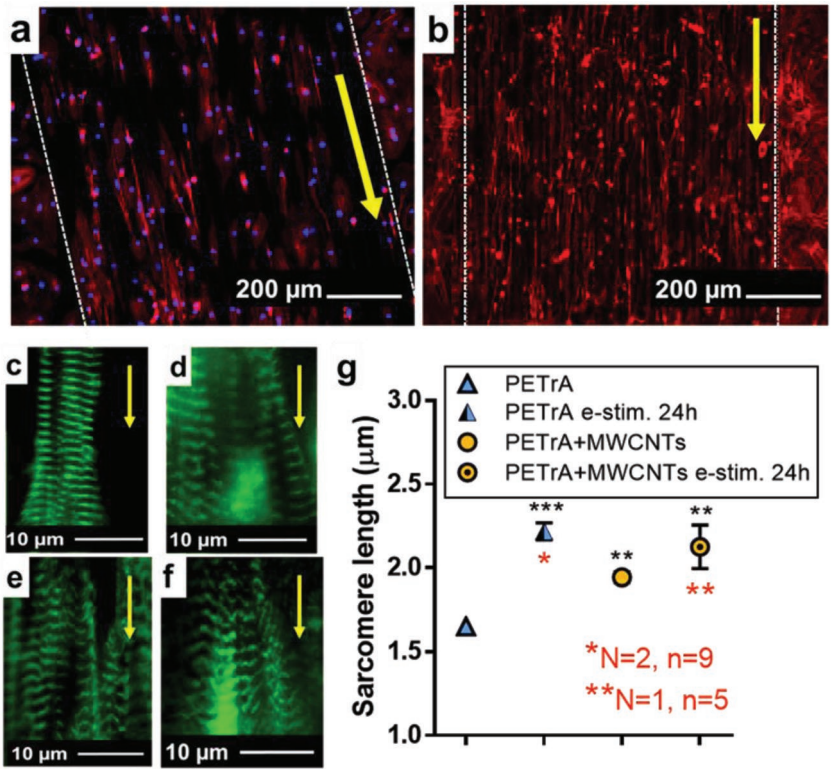

Figure 5. hPSC-CMs cultured on the myofibril-like structure printed using a) pristine PETrA and b) PETrA+MWCNTs. White dotted lines indicate the limits of the structure. Fluorescence microscopic images of sarcomeres of hPSC-CM on myofibril-like structures immunolabeled for cardiac alpha-actinin on c) PETrA, d) PETrA after 24 h electrical stimulation, e) PETrA+MWCNTs, f) PETrA+MWCNTs after 24 h electrical stimulation, and g) their corresponding sarcomere lengths. Electrical stimulation consisted on 2 V at 3 Hz. Yellow arrows indicate direction of microchannels and nanogrooves.

length was observed to increase from 1.65 μm to 2.21 μm (****p*) for the PETrA only structure (Figure 5c–g). This value of sarcomere length was higher than reported in previous studies using bioinstructive polymer cues alone.[3] Interestingly, the sarcomere length of the PETrA+MWCNTs myofibril-like structure without electrical stimulation was 1.94 μm. On comparing the PETrA+MWCNTs myofibril-like structure before and after electro-mechanical stimulation for 24 h, the sarcomere length increased further to 2.12 μm (***p*). Although it was evident that the incorporation of MWCNTs to PETrA contributed to enhancing the hPSC-CMs morphology and structure, after electro-mechanical stimulation, there was no significant difference between the pristine and the composite myofibril structures.

3. Conclusion

In summary, we have shown that the by integrating topographical, biochemical, and electrical cues we could modulate hPSC-CMs phenotype by controlling cell morphology and intracellular ultrastructures. The PETrA and the composite materials developed were noted to promote hPSC-CMs sarcomere organization in serum free conditions. The biomimetic myofibril-like 3D architecture and the presence of MWCNTs further improved this effect. Interestingly, the application of electromechanical stimulus, superseded the sarcomere lengths achieved by topographical cues and the incorporation of conductive material. Yet, the crucial role of the topographical cues in aligning the hPSC-CMs cannot be neglected and thus a combined approach is required to attain directional alignment and phenotypical control of hPSC-CMs. This combined approach of producing complex architectures using cell-maturing materials and wireless delivery of electric field offers the opportunity of engineering biomimetic complex tissues using stem cells for drug assays, tissue engineering and regenerative medicine applications.

4. Experimental Section

Experimental details can be found in the Supporting Information.

Supporting Information

Supporting Information is available from the Wiley Online Library or from the author.

Acknowledgements

J.V. and P.S.A. contributed equally to this work. This work was supported by the Engineering and Physical Sciences Research Council [Grant numbers EP/R004072/1, EP/P027261/1, and EP/N006615/1], British Heart Foundation [Grant numbers SP/15/9/31605, RG/15/6/31436, PG/14/59/31000, RG/14/1/30588, RM/13/30157, and P47352/CRM], and the National Centre for the Replacement, Refinement & Reduction of Animals in Research [Grant numbers CRACK-IT:35911-259146 and NC/K000225/1]. This project received funding from the European Union's Horizon 2020 research and innovation program under the Marie Skłodowska-Curie grant agreement No. 691128. The authors acknowledge the technical assistance offered by the technicians Mark East, Mark Hardy, and Joseph White at the Centre for Additive Manufacturing (CfAM), University of Nottingham. J.V. and P.S.A. would like to thank Ehab Saleh and Christopher Gell, University of Nottingham, for their technical assistance and advice. The authors thank the Nanoscale and Microscale Research Centre (nmRC) for providing access to instrumentation.

Author Contributions: F.J.R., M.A., R.J.M.H., R.D.W., C.J.T., and C.D. conceived, designed and initiated the work. J.V., performed the ink formulation and characterization, design, and 3D printing of the structures. P.S.A. performed the cardiomyocyte differentiation and subsequent cell studies on the printed structures. SC optimized the immunostaining protocol. GR performed Raman analysis of printed structures and analyzed the data. J.L. performed AFM measurements and data analysis of Young modulus calculation. J.T. and L.B. performed early preliminary work on polymer screening for cardiomyocyte attachment. J.V., P.S.A., and F.J.R. wrote the initial manuscript. All authors discussed experiment design and findings. All authors read, commented, and approved the final manuscript.

Conflict of Interest

The authors declare no conflict of interest.

Keywords

3D printing, biomimetic 3D architectures, cardiomyocyte maturation, regenerative medicine

Received: March 8, 2019
Revised: July 6, 2019
Published online:

[1] C. Robertson, D. D. Tran, S. C. George, *Stem Cells* **2013**, *31*, 829.
[2] J. Li, K. Zhu, Y. Wang, J. Zheng, C. Guo, H. Lai, C. Wang, *Mol. Med. Rep.* **2015**, *11*, 815.
[3] A. K. Patel, A. D. Celiz, D. Rajamohan, D. G. Anderson, R. Langer, M. C. Davies, M. R. Alexander, C. Denning, *Biomaterials* **2015**, *61*, 257.
[4] P.-Y. Wang, J. Yu, J.-H. Lin, W.-B. Tsai, *Acta Biomater.* **2011**, *7*, 3285.
[5] H. Sauer, G. Rahimi, J. Hescheler, M. Wartenberg, *FEBS Lett.* **2000**, *476*, 218.
[6] Y. Xia, L. M. Buja, R. C. Scarpulla, J. B. McMillin, *Proc. Natl. Acad. Sci. USA* **1997**, *94*, 11399.
[7] a) V. H. F. Gomes, I. J. SD, N. Raes, I. L. Amaral, R. P. Salomao, L. de Souza Coelho, F. D. de Almeida Matos, C. V. Castilho, D. de Andrade Lima Filho, D. C. Lopez, J. E. Guevara, W. E. Magnusson, O. L. Phillips, F. Wittmann, M. de Jesus Veiga Carim, M. P. Martins, M. V. Irume, D. Sabatier, J. F. Molino, O. S. Banki, J. R. da Silva Guimaraes, N. C. A. Pitman, M. T. F. Piedade, A. M. Mendoza, B. G. Luize, E. M. Venticinque, E. M. M. de Leao Novo, P. N. Vargas, T. S. F. Silva, A. G. Manzatto, J. Terborgh, N. F. C. Reis, J. C. Montero, K. R. Casula, B. S. Marimon, B. H. Marimon, E. N. H. Coronado, T. R. Feldpausch, A. Duque, C. E. Zartman, N. C. Arboleda, T. J. Killeen, B. Mostacedo, R. Vasquez, J. Schongart, R. L. Assis, M. B. Medeiros, M. F. Simon, A. Andrade, W. F. Laurance, J. L. Camargo, L. O. Demarchi, S. G. W. Laurance, E. de Sousa Farias, H. E. M. Nascimento, J. D. C. Revilla, A. Quaresma, F. R. C. Costa, I. C. G. Vieira, B. B. L. Cintra, H. Castellanos, R. Brienen, P. R. Stevenson, Y. Feitosa, J. F. Duivenvoorden, C. G. Aymard, H. F. Mogollon, N. Targhetta, J. A. Comiskey, A. Vicentini, A. Lopes, G. Damasco, N. Davila, R. Garcia-Villacorta, C. Levis, J. Schietti, P. Souza, T. Emilio, A. Alonso, D. Neill, F. Dallmeier, L. V. Ferreira, A. Araujo-Murakami, D. Praia, D. D. do Amaral, F. A. Carvalho, F. C. de Souza, K. Feeley, L. Arroyo, M. P. Pansonato, R. Gribel, B. Villa, J. C. Licona, P. V. A. Fine, C. Ceron, C. Baraloto, E. M. Jimenez, J. Stropp, J. Engel, M. Silveira, M. C. P. Mora, P. Petronelli, P. Maas, R. Thomas-Caesar, T. W. Henkel, D. Daly, M. R. Paredes, T. R. Baker, A. Fuentes, C. A. Peres, J. Chave, J. L. M. Pena, K. G. Dexter, M. R. Silman, P. M. Jorgensen, T. Pennington, A. Di Fiore, F. C. Valverde, J. F. Phillips, G. Rivas-Torres, P. von Hildebrand, T. R. van Andel, A. R. Ruschel, A. Prieto, A. Rudas, B. Hoffman, C. I. A. Vela, E. M. Barbosa, E. L. Zent, G. P. G. Gonzales, H. P. D. Doza, I. P. de Andrade Miranda, J. L. Guillaumet, L. F. M. Pinto, L. C. de Matos Bonates, N. Silva, R. Z. Gomez, S. Zent, T. Gonzales, V. A. Vos, Y. Malhi, A. A. Oliveira, A. Cano, B. W. Albuquerque, C. Vriesendorp, D. F. Correa, E. V. Torre, G. van der Heijden, H. Ramirez-Angulo, J. F. Ramos, K. R. Young, M. Rocha, M. T. Nascimento, M. N. U. Medina, M. Tirado, O. Wang, R. Sierra, A. Torres-Lezama, C. Mendoza, C. Ferreira, C. Baider, D. Villarroel, H. Balslev, I. Mesones, L. E. U. Giraldo, L. F. Casas, M. A. A. Reategui, R. Linares-Palomino, R. Zagt, S. Cardenas, W. Farfan-Rios, A. F. Sampaio, D. Pauletto, E. H. V. Sandoval, F. R. Arevalo, I. Huamantupa-Chuquimaco, K. Garcia-Cabrera, L. Hernandez, L. V. Gamarra, M. N. Alexiades, S. Pansini, W. P. Cuenca, W. Milliken, J. Ricardo, G. Lopez-Gonzalez, E. Pos, H. Ter Steege, *Sci. Rep.* **2018**, *8*, 1003; b) C. Denning, V. Borgdorff, J. Crutchley, K. S. Firth, V. George, S. Kalra, A. Kondrashov, M. D. Hoang, D. Mosqueira, A. Patel, L. Prodanov, D. Rajamohan, W. C. Skarnes, J. G. Smith, L. E. Young, *Biochim. Biophys. Acta* **2016**, *1863*, 1728.
[8] a) E. Huethorst, M. Hortigon, V. Zamora-Rodriguez, P. Reynolds, F. Burton, G. Smith, N. Gadegaard, *ACS Biomater. Sci. Eng.* **2016**, *2*, 2231; b) K. Ronaldson-Bouchard, S. P. Ma, K. Yeager, T. Chen, L. Song, D. Sirabella, K. Morikawa, D. Teles, M. Yazawa, G. Vunjak-Novakovic, *Nature* **2018**, *556*, 239; c) K. Roshanbinfar, L. Vogt, B. Greber, S. Diecke, A. R. Boccaccini, T. Scheibel, F. B. Engel, *Adv. Funct. Mater.* **2018**, *28*, 1803951.
[9] a) S. R. Shin, S. M. Jung, M. Zalabany, K. Kim, P. Zorlutuna, S. B. Kim, M. Nikkhah, M. Khabiry, M. Azize, J. Kong, K. T. Wan, T. Palacios, M. R. Dokmeci, H. Bae, X. S. Tang, A. Khademhosseini, *ACS Nano* **2013**, *7*, 2369; b) W. Xiong, Y. Liu, L. J. Jiang, Y. S. Zhou, D. W. Li, L. Jiang, J. F. Silvain, Y. F. Lu, *Adv. Mater.* **2016**, *28*, 2002; c) S. Ushiba, S. Shoji, K. Masui, J. Kono, S. Kawata, *Adv. Mater.* **2014**, *26*, 5653.
[10] T. J. Kolanowski, C. L. Antos, K. Guan, *Int. J. Cardiol.* **2017**, *241*, 379.
[11] I. Maskery, A. Hussey, A. Panesar, A. Aremu, C. Tuck, I. Ashcroft, R. Hague, *J. Cell. Plast.* **2017**, *53*, 151.
[12] a) D. B. Kolesky, K. A. Homan, M. A. Skylar-Scott, J. A. Lewis, *Proc. Natl. Acad. Sci. USA* **2016**, *113*, 3179; b) J. U. Lind, T. A. Busbee, A. D. Valentine, F. S. Pasqualini, H. Yuan, M. Yadid, S. J. Park, A. Kotikian, A. P. Nesmith, P. H. Campbell, J. J. Vlassak, J. A. Lewis, K. K. Parker, *Nat. Mater.* **2017**, *16*, 303; c) D. Joung, V. Truong, C. C. Neitzke, S. Z. Guo, P. J. Walsh, J. R. Monat, F. Meng, S. H. Park, J. R. Dutton, A. M. Parr, *Adv. Funct. Mater.* **2018**, *28*, 1801850.
[13] Q. Hu, X. Z. Sun, C. D. J. Parmenter, M. W. Fay, E. F. Smith, G. A. Rance, Y. He, F. Zhang, Y. Liu, D. Irvine, C. Tuck, R. Hague, R. Wildman, *Sci. Rep.* **2017**, *7*, 17150.
[14] K. S. Worthington, A. V. Do, R. Smith, B. A. Tucker, A. K. Salem, *Macromol. Biosci.* **2018**, *19*, e1800370.
[15] a) A. Accardo, M.-C. Blatché, R. Courson, I. Loubinoux, C. Vieu, L. Malaquin, *Biomed. Phys. Eng. Express* **2018**, *4*, 027009; b) K. S. Worthington, L. A. Wiley, E. E. Kaalberg, M. M. Collins, R. F. Mullins, E. M. Stone, B. A. Tucker, *Acta Biomater.* **2017**, *55*, 385.
[16] D. Mosqueira, I. Mannhardt, J. R. Bhagwan, K. Lis-Slimak, P. Katili, E. Scott, M. Hassan, M. Prondzynski, S. C. Harmer, A. Tinker, J. G. W. Smith, L. Carrier, P. M. Williams, D. Gaffney, T. Eschenhagen, A. Hansen, C. Denning, *Eur. Heart J.* **2018**, *39*, 3879.
[17] L. H. Nguyen, M. Straub, M. Gu, *Adv. Funct. Mater.* **2005**, *15*, 209.
[18] Y. He, C. J. Tuck, E. Prina, S. Kilsby, S. D. R. Christie, S. Edmondson, R. J. M. Hague, F. Rose, R. D. Wildman, *J. Biomed. Mater. Res., Part B* **2017**, *105*, 1645.
[19] L. Xu, N. Sheybani, W. A. Yeudall, H. Yang, *Biomater. Sci.* **2015**, *3*, 250.
[20] S. Ushiba, S. Shoji, K. Masui, P. Kuray, J. Kono, S. Kawata, *Carbon* **2013**, *59*, 283.
[21] U. Staudinger, G. Zyla, B. Krause, A. Janke, D. Fischer, C. Esen, B. Voit, A. Ostendorf, *Microelectron. Eng.* **2017**, *179*, 48.

[22] a) K. Shapira-Schweitzer, D. Seliktar, *Acta Biomater.* **2007**, *3*, 33; b) B. Bhana, R. K. Iyer, W. L. Chen, R. Zhao, K. L. Sider, M. Likhitpanichkul, C. A. Simmons, M. Radisic, *Biotechnol. Bioeng.* **2010**, *105*, 1148; c) J. G. Jacot, A. D. McCulloch, J. H. Omens, *Biophys. J.* **2008**, *95*, 3479.
[23] X. Yang, L. Pabon, C. E. Murry, *Circ. Res.* **2014**, *114*, 511.
[24] M. C. Ribeiro, L. G. Tertoolen, J. A. Guadix, M. Bellin, G. Kosmidis, C. D'Aniello, J. Monshouwer-Kloots, M.-J. Goumans, Y.-l. Wang, A. W. Feinberg, *Biomaterials* **2015**, *51*, 138.
[25] S. S. Nunes, J. W. Miklas, J. Liu, R. Aschar-Sobbi, Y. Xiao, B. Zhang, J. Jiang, S. Massé, M. Gagliardi, A. Hsieh, *Nat. Methods* **2013**, *10*, 781.
[26] S. Mobini, Ü.-L. Talts, R. Xue, N. J. Cassidy, S. H. Cartmell, *J. Biomater. Tissue Eng.* **2017**, *7*, 829.